LANGMUIR

pubs.acs.org/Langmuir Article

Simultaneous Writing and Erasing Using Probe Lithography Synchronized Erasing and Deposition (PLiSED)

Kexin Jiao,[+] Nathalie Becerra-Mora,[+] Brice Russell, Aldo Migone, Max E. Gemeinhardt, Boyd M. Goodson, and Punit Kohli*

Cite This: https://doi.org/10.1021/acs.langmuir.2c02096 Read Online

ACCESS | Metrics & More | Article Recommendations | Supporting Information

ABSTRACT: Simultaneous writing and erasing of two and three molecules in one single step at the microscale using Polymeric Lithography Editor (PLE) probes is demonstrated. Simultaneous writing and erasing of three molecules was accomplished by rastering a nanoporous probe that was loaded with rhodamine B and fluorescein over a quinine-coated glass substrate. The solvated quinine molecules were erased and transported into the probe matrix, whereas both rhodamine and fluorescein molecules were simultaneously deposited and aligned with the path of the erased quinine on the substrate. The simultaneous writing and erasing of molecules is referred to as PLiSED. The writing and erasing speed can be easily tuned by adjusting the probe speed to as large as 10,000 $\mu m^2/s$. The microscale patterns on the orders of square millimeter area were fabricated by erasing fluorescein with an efficiency (η_e) > 95% while simultaneously depositing rhodamine molecules at the erased spots. The roles of the probe porosity, transport medium, and kinetics of solvation for editing were also investigated—the presence of a transport medium at the probe−substrate interface is required for the transport of the molecules into and out of the probe. The physical and mechanical properties of the polymeric probes influenced molecular editing. Young's modulus values of the hydrated hydrogels composed of varying monomer/cross-linker ratios were estimated using atomic force microscopy. Probes with the highest observed erasing capacity were used for further experiments to investigate the effects of relative humidity and erasing time on editing. Careful control over experimental conditions provided high-quality editing of microscale patterns at high editing speed. Combining erasing and deposition of multiple molecules in one single step offers a unique opportunity to significantly improve the efficiency and the accuracy of lithographic editing at the microscale. PLiSED enables rapid on-site lithographic rectification and has considerable application values in high-quality lithography and solid surface modification.

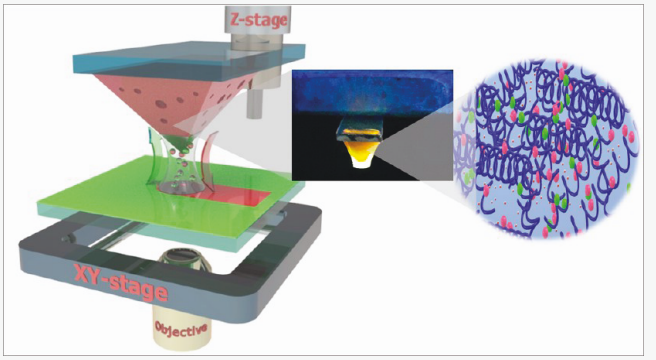

INTRODUCTION

Probe-based lithography is extensively used for delivering and patterning a variety of ink molecules on many types of substrate surfaces.[1] Polymeric lithographic probes are used to deposit dye molecules,[2,3] biomolecules,[4−6] metals,[7] and polymers[8] on a variety of substrates, such as glass,[9] silicon,[10] and polymeric surfaces.[11] The micro- and nanopatterns are then used in biosensing,[6] photolithography,[12] material synthesis,[13] and device fabrication.[7,10] The highest spatial resolution of the probe-based lithographic techniques approaches 15 nm using dip-pen lithography (DPN).[14] Fountain pen nanolithography (FPN) has allowed the deposition of metallic nanoparticles, where the size of the pen/probe nozzle conferred the 15 nm resolution of the technique.[15] Other works have reported patterns within a range of 50 to 100 nm. The use of arrays of DPN probes for multiplex deposition of multiple ink molecules has dramatically increased the nanoscale patterning throughput rate.[12,16−22] An excellent review describing the fundamentals of the scanning probe lithography and its potential applications in a range of fields including materials, life, and medicine is recommended for readers.[23] Most of the studies have been focused on the patterning of a myriad of molecules. However, removal of materials or molecules at the nano- and microscale is relevant as well. Removing molecules from deposited patterns is important for correction and post modification in real lithographic work. Despite its relevance, studies involving error rectification of microscale patterns are scarce in the literature.[24−28] PLiSED is also expected to find applications in areas including energy harvesting, and self-powered and wearable flexible sensors.[29−32]

Received: August 5, 2022
Revised: September 14, 2022

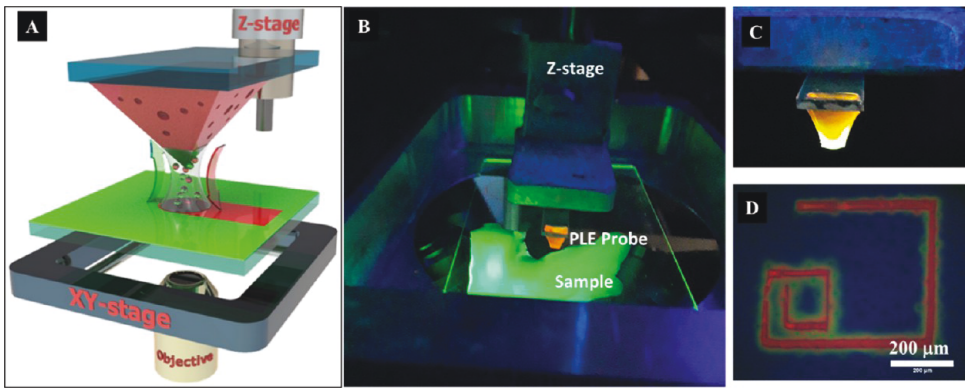

Figure 1. (A) A schematic of PLiSED editing showing editing using two types of fluorescent dyes (green and red). Molecular editing using three types of dye molecules was also demonstrated, but it is not shown in the schematic. A PAAM probe is attached to a *z*-piezoelectric stage, whereas the substrate for molecular editing is placed on an *XY* microscope stage. A meniscus is formed when the probe is in close proximity with the substrate, allowing simultaneous flow of (i) "red" molecules from the probe to the substrate and (ii) "green" molecules from the substrate to the probe. The writing−erasing process is monitored in either bright field or fluorescence mode. (B) A photograph of the setup used for PLiSED. (C) A close view of the probe attached to the *z*-stage. For clarity, a large-scale probe is shown, which is much larger than the microscale probe used for experiments. (D) A spiral pattern fabricated by erasing a blue dye (quinine) and simultaneous deposition of green (fluorescein) and red (rhodamine 6G) dyes on the surface. Three different editing steps were performed in one single step by translocating the fluorescein- and rhodamine-containing PLE tip on a quinine-deposited glass surface.

In general, the removal of molecules from a surface using solution-based probe erasing is a multiple-step process. In the simplest terms, it requires the (1) delivery of an etching and/or a solvating media on a surface; (2) solvation of the targeted species adsorbed on a surface; and (3) transport of the solvated molecules into the probe or away from the erased spot.[26−28] Multiple factors are involved in the removal of molecules from a substrate by a lithographic probe. Some factors are related to the physicochemical characteristics of the material of interest, whereas other factors are associated with the characteristics of the lithographic probe. The physicochemical characteristics of the molecules (including size, charge, shape, and surface energy) and experimental conditions (RH, temperature, and viscosity) may determine the kinetics of the erasing process. Moreover, the solvent content in the matrix of the probe can significantly influence the ink capacity.[33,34]

In our previous work, PLE probes were used for the deposition of fluorescent dyes and removal of metal coatings from planar and nonplanar substrates.[26−28] Pyramidal polyacrylamide probes loaded with copper and silver etchants were used to make electrodes by selectively removing silver or copper from a flat substrate; the electrodes were then used to fabricate a microphotodetector.[27,28] In a similar fashion, conical probes composed of agarose were used to erase fluorescent patterns with an erasing areal speed (R_{edit}) of ≈785 $\mu m^2/s$ and editing resolution of ∼10 μm.[27] For these studies, two steps were required: (a) erasing or removal of a fluorescent dye (rhodamine B) using a swollen probe and (b) writing or deposition of fluorescein, thereby completing the microscale editing. Thus, the editing process required two steps utilizing two different PLE probes, necessitating probe realignment and registration at each step during the patterning process, which can be prone to errors. Furthermore, the sequential multistep process can be cumbersome and time-consuming (lowers editing rate) compared to a process where multiple molecules can be manipulated simultaneously. Therefore, simultaneous erasing and writing of multiple molecules in one step is expected to significantly increase the editing rate because registration and alignment of the probe are needed only once and multiple molecules can be erased and/or deposited in one locomotion step of the probe.

Here, we demonstrate probe lithography synchronized erasing and deposition, referred to as PLiSED, of two and three molecules in one single step. A microscale probe composed of nanoporous polyacrylamide (PAAM) containing one or two types of fluorescent dye molecules was translocated over a substrate coated with one type of fluorescent dye molecules. The solvated molecules on the substrate surface were transported into the probe matrix, whereas fluorescent molecules contained in the probe were transported out of the probe onto the substrate, providing high-quality two- and three-molecular patterning in a single probe locomotion step. The erasing and writing efficiencies of the patterns were >95%. For highly water-soluble fluorescent dyes, $R_{edit} \approx 10{,}000\ \mu m^2/s$ on a millimeter square area was achieved using PLiSED. The combination of erasing and deposition of multiple molecules in one step offers a unique opportunity to enhance the throughput rate, efficiency, and accuracy of the lithographic work. The described technique embodies a potentially powerful addition to the conventional lithographic toolbox for fabrication applications in the areas of nano/microelectronics, electrochemical lithography, and biosensing.

RESULTS AND DISCUSSION

Introduction to the PLiSED Process. Figure 1 shows an overall view of the PLiSED process described in this report. A polyacrylamide (PAAM) probe of microscale dimension loaded with a red dye is rastered over a surface coated with a green dye (Figure 1A); the example shown here is a two-dye PLiSED process. Figure 1B shows the setup used in the experiments. A *z*-axis piezoelectric stage attached to a PLE probe is brought in close proximity to the surface coated with fluorescein. A meniscus formed at the probe−substrate interface allows simultaneous erasing of the green dye and writing of the red dye in one single step. A fluorescent spiral composed of three fluorescent dyes is fabricated in one step by erasing quinine (blue) while writing green (fluorescein) and red (rhodamine) dyes on a glass surface (Figure 1D). A linear editing speed >500 $\mu m \cdot s^{-1}$ and a large editing area (A_e) ∼0.21

https://doi.org/10.1021/acs.langmuir.2c02096
Langmuir XXXX, XXX, XXX−XXX

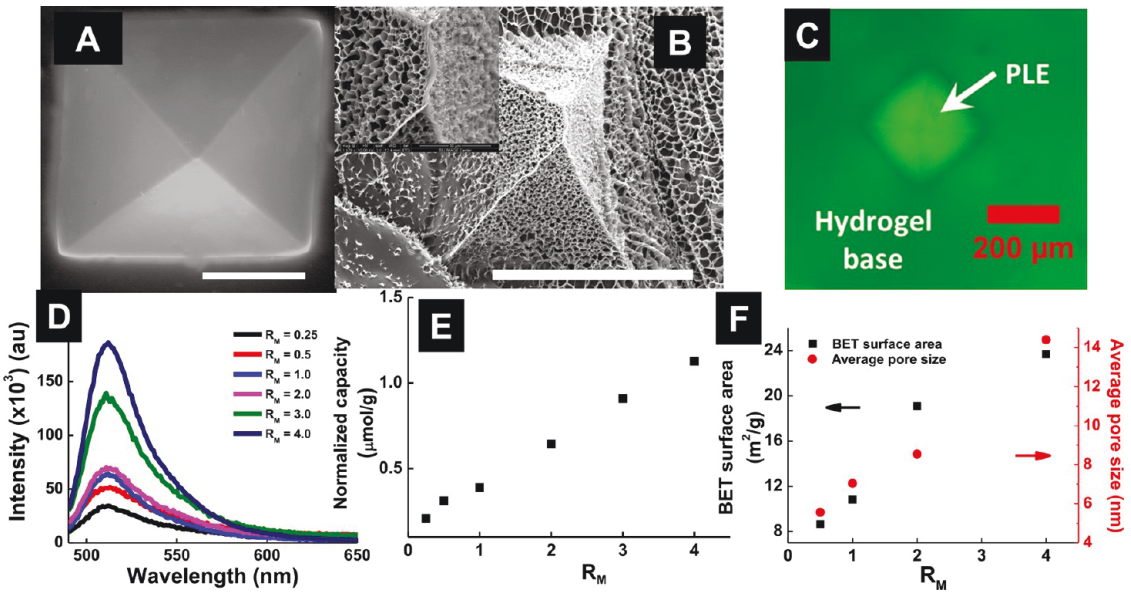

Figure 2. (A) An ESEM image of the top view of a hydrated PAAM PLE with tip size (d_s) ≈ 540 nm and base (d_l) = 125 × 125 μm (scale bar 50 μm). (B) An SEM image of a PAAM probe lyophilized in high vacuum (scale bar 100 μm). (C) A fluorescence micrograph of a fluorescein-loaded PAAM probe showing the tip and base of the probe. (D) Fluorescence spectrum of the extracted solutions from PAAM hydrogels composed with different R_M's. (E) Normalized C_{edit} of PAAM probes composed with different R_M's. (F) BET surface area and pore size of PAAM probes made with different R_M's.

Table 1. PAAM Hydrogel PLE Compositions, Young's Moduli (E), and Maximum Small Molecule Storage Capacity (C_{max})

sample	AAm solution (μL)	bis-AAm solution (μL)	TEMED (μL)	APS solution (μL)	R_M	E (MPa)	C_{max} (cm^3/g)
1	100	100	2	5	1	ND[a]	13.5
2	200	50	2	5	4	0.10 ± 0.04	36.1
3	150	50	2	5	3	ND	26.2
4	200	100	2	5	2	0.84 ± 0.19	17.5
5	100	200	2	5	0.5	0.18 ± 0.04	10.1
6	50	200	2	5	0.25	ND	7.4

[a]ND: not determined.

mm^2 were accomplished using PLE with d_s = 500 nm and d_l = 220 μm. Similarly, we demonstrated simultaneous erasing of quinine (blue) and deposition of rhodamine B (red) and fluorescein (green) in one step using a single PAAM PLE. That is, three individual steps (one erasing and two deposition steps) were combined in a single locomotion step.

Fabrication and Characterization of Polymeric Lithographic Editor (PLE) Probes. Prior to the demonstration of simultaneous probe-based writing and erasing, the probes were characterized using environmental scanning electron microscopy (ESEM), energy dispersive X-ray spectroscopy (EDS), and atomic force microscopy (AFM) for surface roughness and topography, chemical analysis, and mechanical properties. Although conventional SEM can provide high-quality surface roughness and topographical information, it is known to alter material properties and structures of soft materials such as hydrogels at the nanoscale. This limitation is due to the harsh conditions during sample preparation and imaging in SEM.[35] In contrast, ESEM offers the possibility of imaging a hydrogel sample in its hydrated state with minimum changes in its microscale structure.[35,36] Due to these reasons, we imaged PLE hydrogel probes in a hydrated state utilizing ESEM and compared them with images obtained under high-vacuum SEM. The SEM image acquired in high vacuum does not truly represent the actual structure of the probe used for erasing and writing patterns, which showed significant deformation and shrinkage (about 5−7 times that of hydrated probes) (Figure 2B). ESEM micrographs of the PAAM probe depicted a homogeneous and smooth surface. Importantly, the ESEM images of the probes are more likely to resemble the hydrated probes used for molecular editing experiments (Figure 2A).

Surface Area and Porosity of Hydrogel Probes. Knowledge of the surface area, porosity, and mechanical properties of the polymeric probes is important for simultaneous editing of patterns. The capacity of editing depends on the porosity of the probe polymer matrix, whereas the mechanical stiffness of the probes affects the pattern feature size when the probe is in contact with the surface. A higher editing capacity is expected for highly porous PLEs compared to the probes with collapsed pores or nonporous probes (such as PDMS probes). However, the softer probes (i.e., probes composed of lower E) are susceptible to larger deformation under stress and may exhibit larger edited feature size as compared to those patterns fabricated using stiffer probes with larger E.[37] Therefore, depending upon the desired application, a balance between porosity and mechanical properties of the probe material is warranted. Since the monomer/cross-linker ratio controls the mechanical properties, ink storage capacity, and BET surface area of hydrogels composed, investigations of the hydrogels of different values of $R_M = \left(\frac{\text{monomer}}{\text{crosslinker}}\right)$ were performed.

https://doi.org/10.1021/acs.langmuir.2c02096
Langmuir XXXX, XXX, XXX−XXX

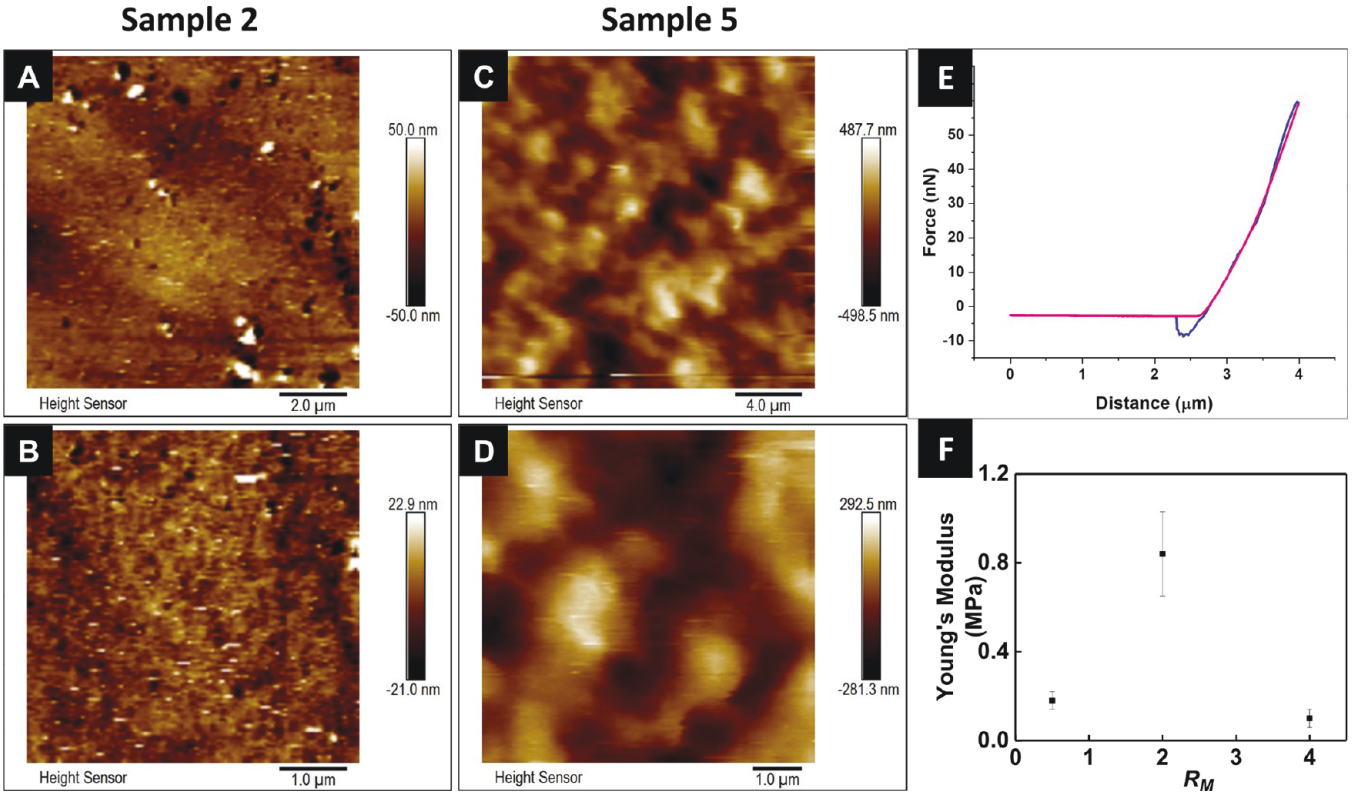

Figure 3. Surface topography and Young's modulus (E) measurements of hydrated PAAM probes. (A) An AFM image of hydrated PAAM probes composed with R_M = 2 and (B) a corresponding AFM at a higher resolution. (C) An AFM image of the hydrogel probe synthesized using R_M = 0.5 and (D) a corresponding AFM image at a higher resolution. (E) Typical force−distance AFM curves of PAAM hydrogel. Red and blue curves are approaching and retracting the AFM tip away from the hydrogel. All the measurements were performed in water. (F) E−R_M dependence of the PAAM probes. The values for E were estimated by measuring the force−distance curves using calibrated probes.

Table 1 and Figure 2 show the ink storage capacity (C_{max}), Young's modulus (E), and BET surface area of the hydrogels composed with different R_M's (Table 1 and Figure 2). C_{max} was estimated by comparing fluorescein emission intensity with a calibration curve and correcting for the dilution factors (Figure S2). The procedure for the estimation of PAAM capacity for storing small molecules such as fluorescein is given in the Supporting Information. The concentration of fluorescein extracted from PAAM hydrogel probes composed with different R_M's was normalized with the weight of each PAAM sample (Figure 2D). The editing capacity of the probes correlated well with R_M. That is, hydrogels composed with an R_M exhibited a higher molecular storing capacity than those hydrogels composed with a smaller R_M. For example, the probes synthesized with R_M = 4 showed the highest capacity ($C_{max} \approx 36.1$ cm^3/g) to store fluorescein in its matrix, which was roughly 5 times larger than the value for probes with R_M = 0.25 exhibiting $C_{max} \approx 7.4$ cm^3/g. The surface area was estimated using nitrogen adsorption measurements according to the BET method.[38] A linear BET surface area−R_M dependence was observed for RM ≤ 4 in our experiments. This trend is not unexpected because softer hydrogels possessed larger surface area (S_{BET}) and larger average pore size (D_p) compared to those for stiffer hydrogels (Figure 2E). This result agrees with the literature where the porosity of PAAM is found to be highly dependent on R_M.[39−41] In a recent study, porous acrylamide and acrylic acid based hydrogels were synthesized, and it was observed that the increase in the cross-linker concentration resulted in a significant decrease in the swelling capacity; however, the mechanical properties (compressive failure) of the gels improved with the cross-linker concentration in the gels.[40]

Young's Modulus of the Hydrated Hydrogels at the Nanoscale Using Atomic Force Microscopy. The stiffness of the PLE probe is a crucial parameter for probe-based writing and erasing. Feature size of the deposited and erased patterns depends upon the applied pressure on the probe, as well as the relative humidity and temperature of the experiments and the stiffness of the probe. Within the linear Hooke's regime ($F = k\Delta d$; $\Delta d \ll$ length of the tip; and k is the cantilever spring constant), the probe tip deformation (Δd) is related to Young's modulus (E) by $\Delta d = \frac{FL_0}{EA}$, where F, L_0, and A are the applied force, original length, and cross-section area of the probe, respectively. Clearly, probe deformation will be smaller for the harder probes (larger E) than for softer probes (smaller E) for the same applied force (F) on the tip. Therefore, control over E of the probe material is important for editing feature size.

For the present work, E was estimated by fitting the force−distance curves to the Sneddon model, which takes into account the interaction of a conical AFM probe with a sample. At least 150 F−d curves were acquired at five different spots for each sample to estimate E values. The data processing was performed using a built-in data processor in Bruker Nanoscope Analysis 2.0. The detailed procedure of E measurements using AFM is described in the Supporting Information.

Figure 3F shows the AFM surface topography and E−R_M dependence of the hydrated PAAM hydrogels in aqueous media, mimicking the state of the hydrogel probes for

https://doi.org/10.1021/acs.langmuir.2c02096
Langmuir XXXX, XXX, XXX−XXX

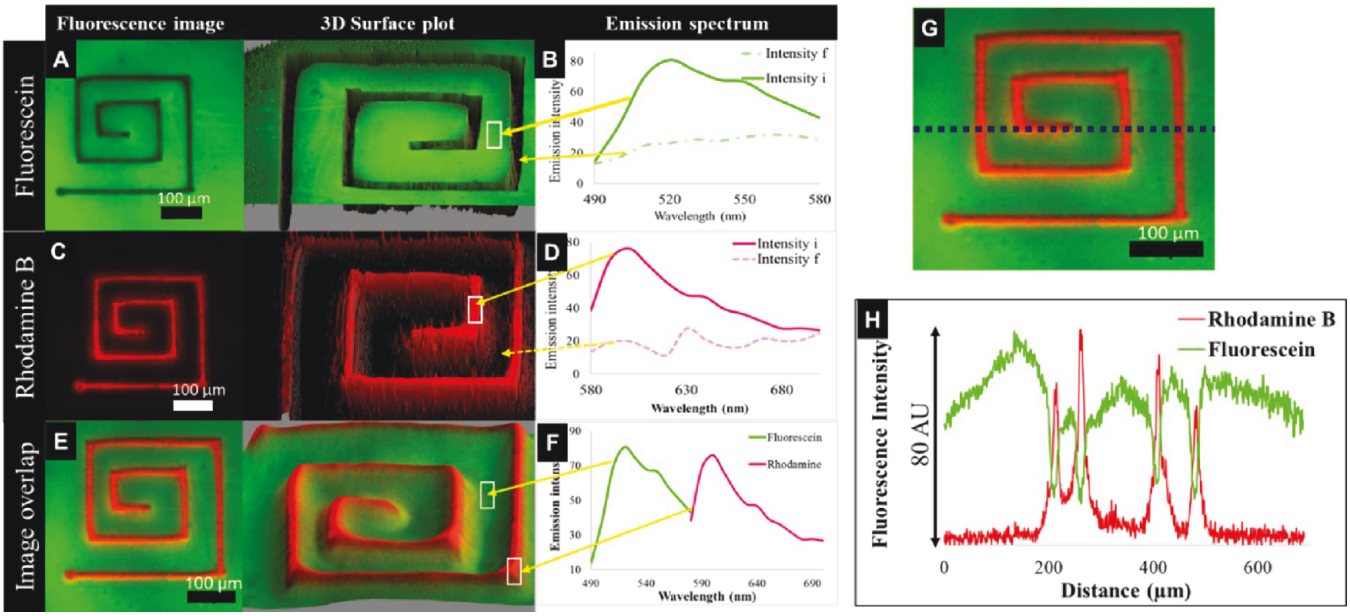

Figure 4. (A) An emission micrograph (left) and 3D surface plot (right) of the spiral fluorescein erasing pattern (green channel). (B) Comparison of the fluorescein emission microspectra at the erased and nonerased microscale spots. (C) An emission micrograph (left) and 3D surface plot (right) of the spiral rhodamine deposition pattern (red channel). (D) Comparison of the rhodamine emission microspectra at the deposited and erased microscale spots. (E) An overlayer emission micrograph of both green and red channels (left) and 3D surface plots (right). (F) Emission spectra of fluorescein and rhodamine emission microspectra at the rectangular box in (E). (H) Emission intensity−distance profile along the dotted gray line of the micrograph in (G). Fluorescein and rhodamine B gray intensity is shown in green and red, respectively. The minimum gray intensity values of the green color profile was for the erased fluorescein where rhodamine B (red profile) showed higher intensity demonstrating spatial overall of erased and deposited molecules using PLiSED. The scale bar is 100 μm; v_{stage} = 5 μm/s; T = 22 °C; and RH = 40%.

molecular editing. E values are averages of 10 different points randomly chosen on the PAAM samples. Figure 3E shows typical force−distance curves of the AFM measurements performed in water. The approach and retracting of the tip are shown in red and blue curves, respectively. As expected, E of the hydrogels was influenced by R_M. E of the hydrogels was found to increase with R_M, but a reduction in the E for the matrix composed with R_M = 4 was observed (Figure 3F). For example, the samples composed with R_M = 2 exhibited E = 0.84 ± 0.19 MPa, which was more than 8 times and 5 times the E values for R_M = 0.5 and 4, respectively. It is reported that the cross-linker concentration above a threshold for the PAAM hydrogel can lead to polymers with uneven cross-linking density in the matrix, where highly cross-linked and poorly cross-linked polymer clusters coexist within the polymer matrix.[42,43] Non-uniform cross-linking density in the matrix with local heterogeneity is thought to be responsible for the observed softening of the hydrogels at higher cross-linker concentrations.[42,43] From a practical perspective, both the capacity and rigidity of the PLE probes are crucial to editing for a desired application. Some applications may require a smaller feature size without a need for a large editing area. For these applications, stiffer probes are preferred, whereas softer probes with a larger capacity are preferred for applications requiring larger editing areas. For all studies performed in this report, the PAAM PLE probes composed with R_M = 2 were selected because of their high capacity and stiffness values.

Patterning Using PLiSED. The simultaneous pattern editing experiments were performed on an inverted microscope equipped with a computer-controlled *XYZ* stage as outlined in previous reports (Figure 1 and the Supporting Information).[26,27] PLiSED was accomplished by bringing the PLE probes containing two types of fluorescent molecules (concentrations in the micromolar range) in close proximity with a substrate coated with a third fluorescent dye. The rapid diffusion of molecules from the nanoporous PAAM probe matrix to the substrate (writing or deposition step) along with the simultaneous diffusion of the solvated molecules adsorbed on the substrate into the PLE probe matrix (erasing step) resulted in PLiSED. For example, the erasing of fluorescein molecules on substrates was accomplished by diffusion of solvated fluorescein molecules into the PLE matrix (Figure 4A). Similarly, the solvated rhodamine B molecules (5.5 μM) trapped within the PLE matrix were simultaneously deposited at the erased patterns (Figure 4B). Fluorescence micrographs and emission spectra of the deposited and erased spiral patterns are shown in Figure 4. The quality of writing and erasing processes was confirmed by the emission microspectra before and after deposition and erasing, respectively. A strong fluorescein emission maximum centered at $\lambda_{em} \approx$ 515 nm (green channel) on nonerased spots and a large decrease in its emission intensity on the erased spots confirmed high-quality erasing using a PAAM probe (Figure 4B). Similarly, the strong emission at $\lambda_{em} \approx$ 590 nm from rhodamine B at the deposition spots (Figures 4C,D) confirmed simultaneous writing and erasing in one single probe locomotion step (Figures 4E,F). A more careful analysis of the FWHM of the gray intensity values for rhodamine B and fluorescein yielded similar pattern sizes of the erased and deposited patterns (Figure S3 and Table S1). Whereas the width and the area of the erased fluorescence pattern in the green channel were 35 ± 11 μm and ~100,000 μm^2 (n = 5, Table S1), respectively, the width and area of the rhodamine B patterns deposited at the fluorescein erased pattern areas were 36 ± 13 μm and ~98,000 μm^2 (n = 5, Table S1), respectively (Figure 4G). The superimposed emission spectra and matched spatial registrations of fluorescein and

https://doi.org/10.1021/acs.langmuir.2c02096
Langmuir XXXX, XXX, XXX−XXX

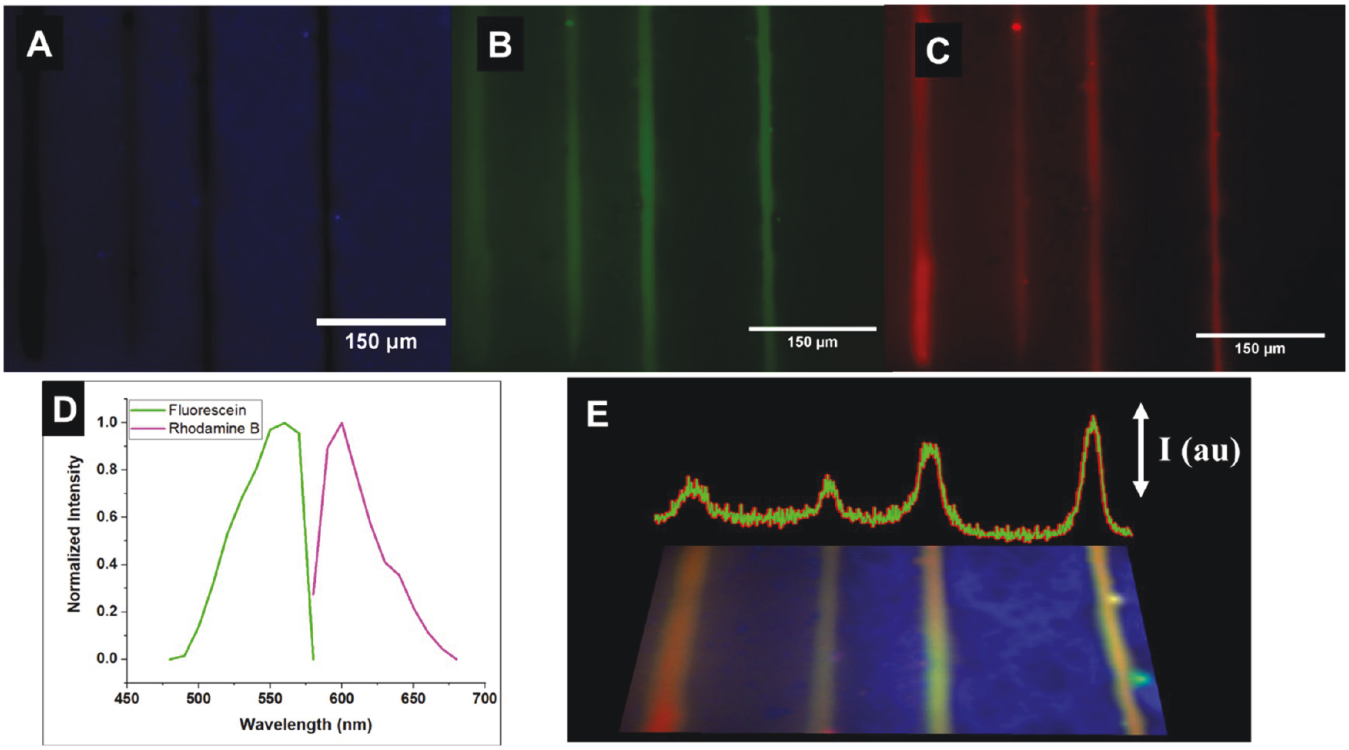

Figure 5. (A) Fluorescent image showing erasing of quinine and simultaneous deposition of (B) fluorescein and (C) rhodamine B. (D) Emission spectra of the fluorescent micrograph in (E) showing deposition of fluorescein (green curve) and rhodamine B (red curve). The emission from quinine was below the detection limit of the hyperspectral camera. (E) An overlapped image composed of three emission channels: blue (quinine), green (fluorescein), and red (rhodamine B). Emission intensity−distance dependence for fluorescein (green curve) and rhodamine (red curve) is also shown. The long pass filters were used for fluorescence emission acquisition. For the blue channel: excitation wavelength (λ_{ex}) = 360−390 nm, emission wavelength (λ_{em}) = 435−720 nm; green channel: λ_{ex} = 465−495 nm, λ_{em} = 515−720 nm; and red channel: λ_{ex} = 532−557 nm, λ_{em} = 570−720 nm. The probes were soaked in fluorescein and rhodamine B solutions of 35 and 5.5 μM, respectively. All the scale bars are 150 μm; v_{stage} = 5 μm/s; T = 22 °C; and RH = 40%.

rhodamine patterns confirmed the successful simultaneous erasing of fluorescein and deposition of rhodamine B without significant distortion (Figure 4H).

PLiSED of three different dyes in one probe locomotion was also accomplished by erasing quinine and simultaneous deposition of fluorescein and rhodamine B on the erased patterns in a single step (Figure 5). A PAAM PLE loaded with fluorescein (35 μM) and RHB (5.5 μM) was brought in close proximity to a glass substrate coated with quinine (146 μM). In this case, instead of a spiral pattern, four parallel lines were fabricated (RH = 40%, temperature = 25 °C, and d_s = 1 × 2 μm). A significant decrease in the emission signal in the blue channel from the quinine dye was observed, whereas both the green and red emission signals significantly increased by many orders at the erased spots, confirming the high selectivity and accuracy of the PLiSED (Figure 5 and Table S2). The feature sizes of the erased and deposited patterns were similar, although some disparity in the width of the emission signals of green and red was observed (Figure 5 and Table S2). The dimensions of the patterns were 9.7 ± 0.9 μm (quinine erasing), 15.0 ± 1.0 μm (fluorescein deposition), and 13.6 ± 1.8 μm (rhodamine deposition), respectively (Table S2). The differences in the deposited patterned line widths were attributed to differences in the probe−surface contact area and the physical and chemical characteristics of the fluorescent dyes involved in the molecular editing process.[26] In general, a larger probe−surface contact area results in a wider pattern feature size. Similarly, the physical and chemical properties of the fluorescent molecules can also influence the dimension of the erased and deposited patterns. For example, the charge and size of the molecules and surface energy differences between the solvent and substrate affect the size of the patterns.[26] When aqueous-based molecular deposition was performed on low-surface-energy surfaces (hydrophobic and fluorinated surfaces), the observed deposition patterns were sharper with a high contrast value, and the pattern feature size was also smaller than for the molecular deposition on high-surface-energy surfaces (hydrophilic surfaces).[26] Therefore, the observed pattern dimension differences were attributed to the local surface-energy differences.[26]

Effect of Probe Porosity and the Presence of a Transporting Medium on Writing and Erasing Patterns. In general, the presence of a transport medium (i.e., meniscus) at the substrate−probe interface is required for probe-based pattern editing.[26,27,44] In the present studies, the quality of pattern editing was found to be highly dependent upon the porosity of the probes and solvent content in the probe matrix. A series of experiments were performed using hydrated and lyophilized PAAM and PDMS PLE probes to investigate the effects of probe porosity and solvent in the matrix on pattern editing. The comparison of the quality of the pattern editing using hydrated PAAM and nonhydrated PLE probes provided useful information regarding the effect of solvent in the matrix on the pattern editing. The freeze-dried and nonporous PDMS probes yielded limited capacity for molecular patterning, whereas the wet porous probes allowed high-quality microscale

https://doi.org/10.1021/acs.langmuir.2c02096
Langmuir XXXX, XXX, XXX−XXX

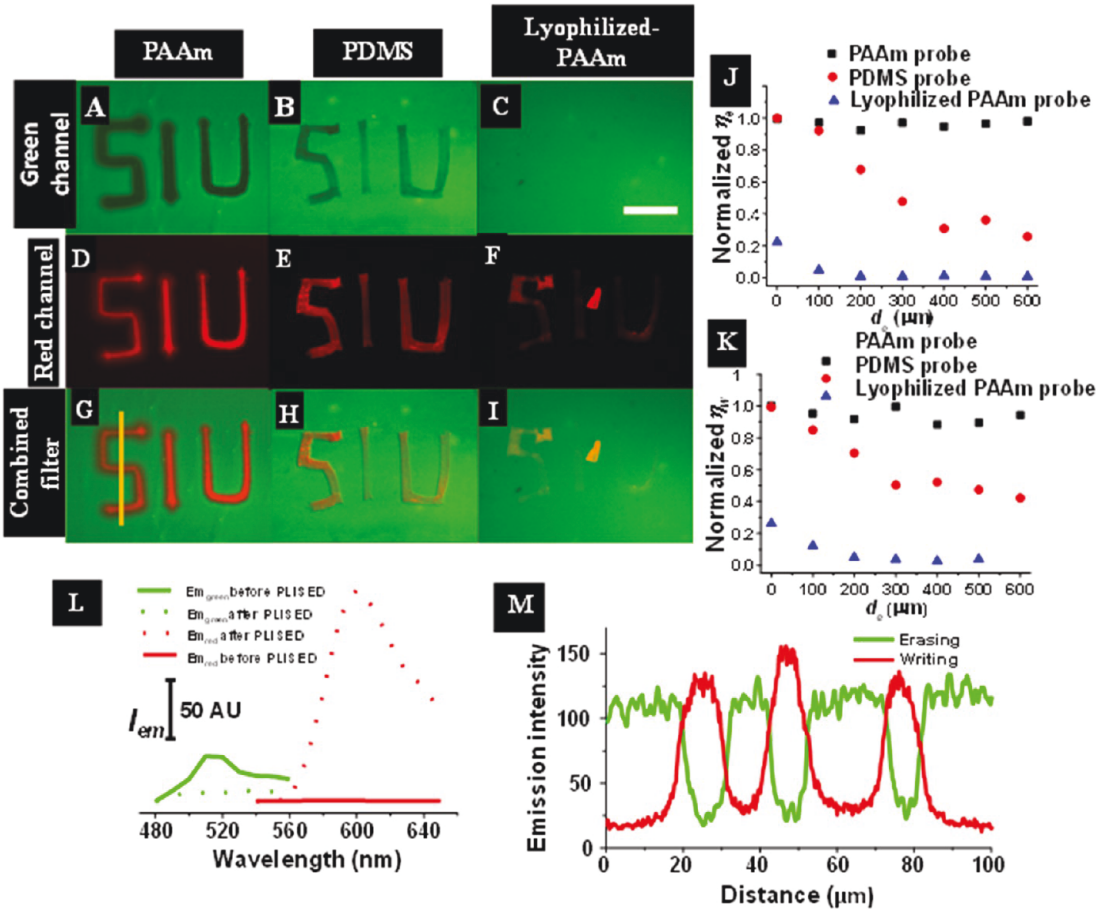

Figure 6. PLISED using hydrated PAAM, PDMS, and lyophilized PAAM PLEs. (A–C) Erasing of fluorescein (green channel); (D–F) simultaneous deposition of rhodamine B (red channel); and (G–I) the overlap of green and red channels of :″SIU″ simultaneous editing using three different PLE probes. (J) Erasing efficiency (η_e)–distance dependence of ″S″ in (G). (K) Writing efficiency (η_w)–distance dependence of ″S″ along yellow line in (G). (L) Fluorescence spectra fluorescein (in A) and rhodamine B (in D) at the microscale before and after PLiSED using a hydrated PAAM PLE. (M) Line scan of the erased pattern using a hydrated PAAM PLE in (G). The emission intensity for red and green channels in (M) corresponds to the yellow line in (G). The probe with a tip size of 1 × 2 μm was used for all experiments (RH = 40% and T = 22 °C). Scale bar for all micrographs is 50 μm.

editing of large areas (>0.2 mm^2) with ease. This was accomplished by measuring the erasing (η_e) and writing efficiency (η_w) for hydrated PAAM, lyophilized PAAM, and PDMS probes. η_e and η_w are defined as

$$\left(1 - \frac{I_0}{I_t}\right) \quad (1)$$

and

$$\left(1 - \frac{I_t}{I_0}\right), \quad (2)$$

respectively. Here, I_0 and I_t represent the fluorescence emission intensity before and after pattern editing, respectively. For all experiments, probes (tip size = 1 × 2 μm) were immersed in a 1 μM rhodamine B solution for 2 h prior to use (RH = 40% and temperature = 22 °C). The editing process using lyophilized PAAM PLE was similar to the hydrated PAAM probe except that the PAAM probe was first swollen in 1 μM rhodamine B solution for 2 h prior to lyophilization overnight. This procedure yielded rhodamine-containing lyophilized PLE probes but without solvent in the probe matrix.

The hydrated PAAM PLE provided the highest quality for the PLiSED out of three types of probes investigated in our experiments (Figure 6). A fluorescence intensity line scan of ″SIU″ fabricated using a hydrated nanoporous PLE probe showed a sharp decrease in the green emission intensity (Figure 6A) and simultaneous increase in the red emission in ″SIU″ (Figure 6B). At every 100 μm, the η_e and η_w were estimated using eqs 1 and 2 and are plotted in Figure 6J,K, respectively. The η_e and η_d for hydrated PAAM probes remained constant for erasing and writing for a distance (d_e) of 600 μm (Figure 6J,K). The emission spectra of fluorescein at the erased areas were below the detection limit of the multispectral camera (green dotted spectrum in Figure 6L), whereas the emission spectra of rhodamine B increased many orders of magnitude after writing (red dotted spectrum in Figure 6L), confirming the high-quality simultaneous fluorescein removal and rhodamine B deposition by the hydrated porous PLE probe. Furthermore, the excellent spatial alignment of the reduction in the green channel intensity and concurrent increase in the emission intensity in the red channel suggested that minimum spreading of the deposited molecules on the surface was incurred (Figure 6M). Overall, both the spectroscopic and spatial observations indicated that high-

https://doi.org/10.1021/acs.langmuir.2c02096
Langmuir XXXX, XXX, XXX–XXX

Scheme 1. Various Steps Involved in Sequential Writing (eq 3), Sequential Erasing (eq 4), and PLiSED (eq 5) Processes[a]

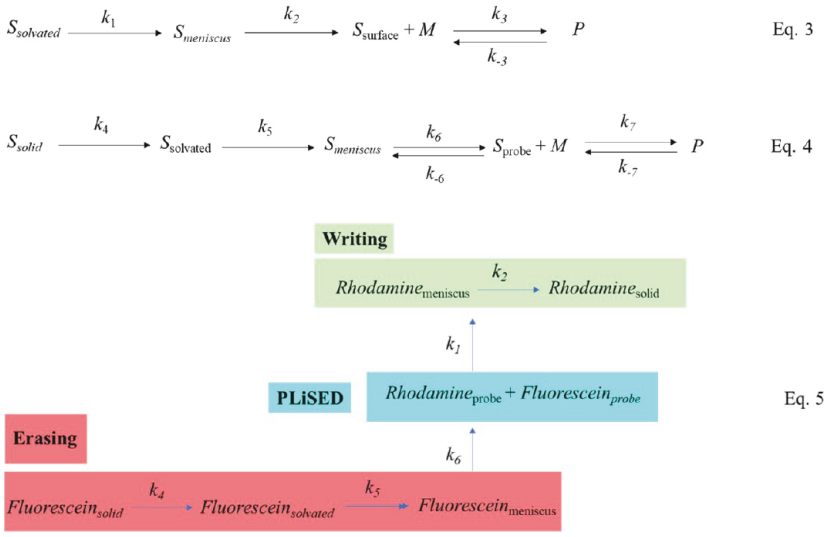

[a]Red and green shaded texts in eq 5 denote erasing and writing processes (respectively), whereas blue shaded text denotes writing and erasing molecules in the probe.

quality PLiSED was accomplished in one single step using hydrated nanoporous probes.

On the other hand, the η_e and η_d values for a lyophilized PAAM PLE were close to zero. These observations confirmed that the transport of molecules into and out of the probe was negligible for lyophilized PLE probes (Figure 6C,F,I,J,K). Similarly, the η_e and η_d for the rhodamine B impregnated PDMS probe decreased from 1.0 ($d_e \approx 0$ μm) to 0.5 ($d_e \approx 300$ μm). Microscale spectroscopic evidence of the erased fluorescein was also obtained using a multispectral camera. The comparison of writing and erasing performed using three different probes suggested that lyophilized PAAM probes exhibited the lowest quality of erasing and writing in our experiments (Figure 6C,F,I). The lack of transporting water molecules in the lyophilized probes resulted in an almost complete absence of (for lyophilized PAAM) and significantly reduced (for PDMS) transporting media at the probe−substrate interface for erasing and writing processes. These results are consistent with probe-based deposition[9,44] and editing studies,[26,27] where the role of the transporting medium at the probe−substrate interface has been shown to require transporting molecules between probe and substrate.

These experiments also highlight the significance of the porosity of the probes for storing the ink molecules in the probe matrix for molecular editing. The surface area (SA) of a nonporous PDMS PLE with a base diameter of 200 μm and height of 85 μm was estimated to be 0.22 μm^2, whereas the experimentally measured BET surface area of a PAAM PLE fabricated using the same Si template was ~22 m^2/g (Figure 2F). Therefore, the theoretical capacity of the nanoporous lyophilized PAAM probe is many orders larger than that of the PDMS probe, which contributed to large differences in the observed η_w and η_e. The thickness of the hydration for the lyophilized PAAM is a few nanometer thick water layers at RH = 10−90%,[45] implying that the capacity of the lyophilized PAAM to contain solvated rhodamine molecules in the lyophilized PAAM matrix is rather limited as compared to fully hydrated PAAM probes. In practice, however, the observed capacity for the hydrated PAAM probes is much larger than that for lyophilized probes because the solvated ink molecules were also contained in the solvent-filled pores, providing a much larger quantity of ink molecules for writing and erasing.

Another consequence of the lack of solvent water meniscus at the interface is the increase in the friction between the probe and surface during probe locomotion. The PLiSED probe shape was distorted during probe movement when it was in contact with the surface. The result of this shape change effect is clearly seen in Figure 6B,E,H, where highly distorted writing and erasing were observed with the PDMS probes. In contrast, patterns fabricated using hydrated PAAM probes were devoid of distortion at the microscale. These results are consistent with our previous observations where the locomotion of the hydrated probes allowed fast high-quality pattern formation.[26,27] Finally, the transport of molecules on PDMS PLE probes is dominated by surface diffusion, which is a much slower process than the molecular diffusion in the hydrated state. For example, the diffusion coefficient (D) of fluorescein in PAAM hydrogel pores is 3.9×10^{-6} cm^2/s[46] (which is close to that of the bulk diffusion coefficient of 4.33×10^{-6} cm^2/s), whereas the reported surface diffusion coefficient of fluorescein on PDMS is ($\sim 7 \times 10^{-8}$ cm^2/s),[47] about 2 orders smaller than that for the hydrated PAAM matrix. Overall, the role of transporting media and porosity of the probe is crucial to molecular editing of the patterns at the microscale level, and careful attention to these parameters is needed for a desired application.

Differences between Probe-Based Writing and Erasing. It is important to consider differences between probe-based *sequential* erasing and writing processes and *simultaneous* writing and erasing processes. In general, writing or deposition of molecules using a probe is a simpler process than erasing (or etching) of materials from a surface (Scheme 1). The deposition of a species S *via* a diffusion mechanism (or an active transport mechanism[48]) involves solvated species ($S_{solvated}$) from the probe matrix to a substrate (eq 3). The molecular species within the probe matrix are usually in the solvated form. Equations 3−5 describe writing (eq 3), erasing (eq 4), and simultaneously writing and erasing (eq 5) steps. Although the deposition of ink molecules can involve more

https://doi.org/10.1021/acs.langmuir.2c02096
Langmuir XXXX, XXX, XXX−XXX

complicated processes, in the simplest sense for the deposition or writing step, k_1 is the transport rate of solvated molecules from the probe to meniscus through the diffusion mechanism, k_2 is the rate constant for $S_{solvated}$ to the surface through a meniscus at the probe−surface interface, and k_3 and k_{-3} are forward and backward rate constants of adsorption and dissolution of $S_{solvated}$ on the surface, respectively. The solvated species either will deposit without reaction with other species (M) present on the surface or may react with M to form a product (P) (eq 3).

Similarly, for the erasing process, the first step involves solvation of a species S adsorbed (or absorbed) on the surface to a $S_{solvated}$ species with a rate constant of k_4. This is followed by diffusion of the $S_{solvated}$ into the probe matrix with a rate constant of k_5. Finally, the reaction of $S_{solvated}$ with M to P can occur with an apparent equilibrium constant of $\frac{k_6}{k_{-6}}$ (eq 4). Thus, in the simplest terms, the probe-based sequential erasing and writing involves a total of seven or more steps (eqs 3 and 4). Because of the high concentration gradient from the probe to the substrate, k_1, k_2, k_4, and k_5 are assumed to be uniforward direction. However, the reverse transport rate constants (k_{-1}, k_{-2}, k_{-3}, and k_{-4}) can be appreciably high for large area editing applications, where the concentration of the erased molecule present at the probe tips can be high (that is, the concentration gradient between the substrate and probe tip is low). Under these circumstances, the reverse rate constants need to be considered and may not be neglected.

For the PLiSED process, the steps in eqs 3 and 4 occur simultaneously within the time scale of our experiments (that is, eq 5) through the locomotion of the probe. Here, the reaction steps in the red shade denote erasing of fluorescein deposited on a surface, whereas the green shade represents deposition of the solvated rhodamine into the probe matrix through the meniscus. The steps shown in eq 5 provide a simplistic overall view of the simultaneous editing process. The diffusion coefficients of rhodamine and fluorescein in water are $\sim 3.5 \times 10^{-6}$ cm^2/s,[46] and the fact that both fluorescein and rhodamine are highly water soluble (i.e., k_4 is fast) allows both writing and erasing of soluble dyes within the time scale of the experiments. However, depending upon the species in editing involved, some steps in eqs 4 and 5 can be slow. Although, Cu^0 can be erased using concentrated acidic $FeCl_3$ in the experimental timescale, the solvation of sputtered copper metal (Cu^0) on chromium-containing glass wafer using an acidic $FeCl_3$ etchant is a kinetically slower process than the solvation of the physisorbed dye molecules on a glass surface. Here, the reaction of etchant molecules with metal atoms adhered strongly to a surface may involve multiple steps for the solvation of Cu^0 into the solution phase.[49,50] Furthermore, the etching of Cu^0 with acidic $FeCl_3$ also involves multiple ferric and ferric-hydrate species in the solution phase whose diffusion coefficient and transport rates can vary significantly in bulk and within the hydrogel matrix. For example, the dominant species in a concentrated aqueous solution of $FeCl_3$ is a trans-$[FeCl_2(H_2O)_4]^+$ complex along with $[Fe(H_2O)_6]^{3+}$ and $[FeCl(H_2O)_5]^{2+}$, whereas hydrated Fe^{3+} and chloride ions are the dominating species in the dilute aqueous $FeCl_3$ solutions.[51]

Large-Scale PLiSED. The hydrated nanoporous probes allowed microscale editing of mm^2 area with high editing speeds (editing speed = width of probe × speed of the probe) of >500 μm^2/s. Such high editing speeds require careful monitoring of the editing quality of the patterns. The editing quality (r_e) is a quantitative measure of simultaneous erasing and writing during probe locomotion. r_e was estimated by quantifying the amount of fluorescein dye molecules absorbed into the PLE matrix after editing trials for different editing areas. The linear speed of the editing was 100 μm·s^{-1}, and the stage was moved in an ″S″ shape loop with 1 and 5 μm step intervals along the x and y directions, respectively (Figure S5G). The total editing area was 0.22 mm^2 for these experiments where fluorescein was erased and rhodamine was deposited simultaneously. Interestingly, the r_e value was found to depend upon the editing area (A_e) of the micropattern (Figure S5H). The r_e−A_e curve showed a sharp decrease in r_e for $0 \le A_e \le 0.01$ mm^2 followed by a plateau for the 0.05 mm^2 $\le A_e \le$ 0.25 mm^2 region. Such a large decrease in the editing rate is likely due to multiple factors, including the physical characteristics of the probe and the molecular capacity of the probe within its matrix. The probes used in these editing experiments were either pyramidal or conical in shape with a typical probe tip area of ∼2 μm^2. The tip area is more than 10^5 smaller than the total editing area in the experiments (0.22 mm^2). Importantly, the probe tip possessed a limited free volume (unoccupied free space), which increases with d^3 where d is the distance away from the tip. In the beginning of the editing process ($0 \le A_e \le 0.01$ mm^2), the unoccupied void space at the PLE tip allows the fast diffusion of fluorescein into the PLE matrix and rhodamine out of the matrix. However, the limited pore volume of the probe tip acts as a bottleneck for the transport of the dye molecules for large editing ($A_e \ge 0.5$ mm^2). For $A_e > 0.05$ mm^2, the molecular transport rate plateau likely indicates a dynamic equilibrium between the erased molecules transported into the probe tip and those depositing ink molecules diffusing out of the probe matrix. Here, the molecular diffusion at the probe tip vicinity occurs in two different directions. The first path involves the diffusion of rhodamine from the probe tip to the surface through the interfacial meniscus, and the second path is the diffusion of the solvated fluorescein molecules present in the meniscus into the probe matrix. Interestingly, the diffusion coefficients of small molecules such as fluorescein and rhodamine in bulk and gels are of similar orders of magnitude,[46,47] suggesting that the transport of fluorescein and rhodamine molecules is comparable within the pores of the probe and in the bulk solution and that there is little or no impediment of the transport of the molecules in the probe matrix for the dilute dye solutions used in our experiments. There is some possibility of competition between depositing and erasing molecules for the sites (free volume) within the probe matrix for simultaneous writing and erasing. However, for dilute solutions and highly porous probes such as those used here, the competition for sites in the probe matrix may not be a significant concern. On the other hand, the highly concentrated solution in the probes with limited porosity (such as those of PDMS probes) of very narrow pores can be a concern as it will reduce the diffusion coefficient of both the erased and deposition molecules in the probe matrix.[52] A minor point also worth mentioning here is that the overall molecular storage capacity for one-step PLiSED is comparable to that of the sequential microscale erasing and writing performed in different steps.

Erasing the Feature Dimension (d_t)−Dwelling Time (τ_e) Relationship. A PAAM PLE with a line shape tip (1 × 2 μm) containing 40% w/w water was used to study d_t

https://doi.org/10.1021/acs.langmuir.2c02096
Langmuir XXXX, XXX, XXX−XXX

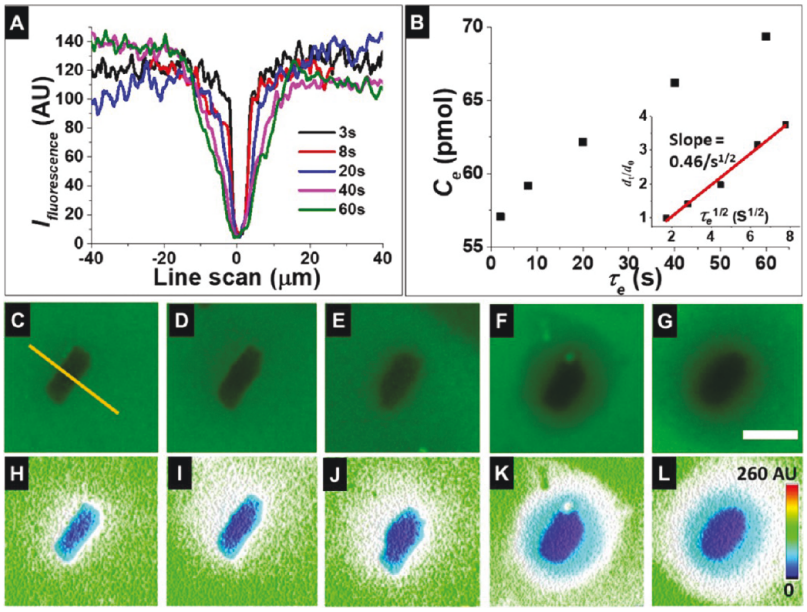

Figure 7. (A) Line scans of erased patterns with different τ_e. (B) Plots of the amounts of fluorescein molecules absorbed by PAAM PLE with different τ_e. Inset in (B) shows the plots of d_t/d_0 (A) as a function of $\tau_e^{1/2}$. Here, d_0 and d_t are FWHM of the emission−distance curves at τ_e = 3 s and t, respectively. (C−G) Optical images for erased pattern with different τ_e. (H, I) Corresponding 3D intensity plots shown in (C−G), respectively. The τ_e values for (C, G) are 3, 8, 20, 40, and 60 s. Scale bar = 10 μm for (C−L). RH = 40% and T = 22 °C for all experiments.

dependence on τ_e (RH = 40%, T = 22 °C). We estimated d_t and d_0 by measuring the full width at half-maximum (FWHM) of the intensity−distance dependence at $\tau_e = t$ and τ_e = 3 s, respectively. The fluorescein-coated surfaces were synthesized by spin coating 20 μL of 1 μM fluorescein disodium salt solution on a glass cover slip at 5000 rpm for 30 s. A hydrated PAAM PLE probe attached to a z-piezoelectric motor was made to contact with a fluorescein-coated glass substrate. The η_e was estimated for the probe−substrate contact area (A_e) of ~56 μm^2 (5.2 × 10.8 μm) with dwell time (τ_e) in the range of 3 s ≤ τ_e ≤ 60 s. Figure 7A shows line scans acquired in the center of each erasing pattern. The line emission scans showed a flat emission baseline in the nonerased area indicating a lack of erased fluorophore molecules on these areas on the surface. Assuming that the intensity of the fluorescence is proportional to the number of molecules in the erased area, a high-quality erasing with η_e > 95% was observed (τ_e = 3 s) (Figure 7C). However, the periphery of the erased patterns (τ_e > 20 s) showed significantly reduced contrast, indicating a lower η_e than that at the center of the erased patterns (Figure 7E−G). One reasonable explanation for the degraded peripheral erasing is that the molecular erasing at the periphery of the patterns was primarily accomplished through the diffusion of fluorescein molecules through the meniscus formed at the tip−surface interface where the probe matrix was not in intimate contact with the surface. This is a consequence of the incomplete transport of the solvated fluorescein molecules into the matrix, where a fraction of the solvated fluorescein molecules remained on the surface after erasing, resulting in a reduced η_e value. Although this process allowed erasing of the ink molecules, the quality of molecular erasing was however significantly deteriorated when compared to erasing patterns at τ_e = 3 s.

A linear relationship between the number of moles of fluorescein erased (C_e) with τ_e was obtained in erasing experiments with an erasing rate of ~0.11 pmol/μm^2s (Figure 7B). The $(\frac{d_t}{d_0})-\sqrt{\tau_e}$ linear relationship indicates that the erasing process is diffusion controlled where the solvated fluorescein molecules were driven into the PLE matrix through a concentration gradient between molecules absorbed on the surface and in the probe matrix. $(\frac{d_t}{d_0})$ denotes a dimensionless normalized erasing pattern parameter, where d_t and d_0 are the FWHMs of the erased patterns for $\tau_e = t$ and undeformed probe dimension, respectively. $(\frac{d_t}{d_0})-\sqrt{\tau_e}$ dependence agrees well with previous studies where it was demonstrated that control over τ_e is an important parameter for high-quality pattern editing without excessive erasing in the undesired region, especially at the periphery of the erased patterns.[27]

Influence of Humidity on Erasing Quality. The local humidity in the vicinity of the probe tip can greatly influence the molecular deposition rate and quality of the patterns.[27,44] With all parameters held constant, molecular erasing was performed at three different RH values of 40, 70, and 95% to investigate the effect of RH on the microscale patterning (Figure 8). These RH conditions represent moderate (40%) to high (90%) humidity conditions encountered in laboratories. To quantify the erasing quality, the quantity of ink erased (C_e) was measured at different RH experiments using a PAAM probe. The estimated erasing rate $(\frac{\partial C_e}{\partial t})$ was 0.21, 0.44, and 0.67 pmol/μm^2·s for RH = 40, 70, and 95%, respectively (Figure 8A). Not surprisingly, both the C_e and FWHM of the erased patterns increased with RH. A quality factor, $W_r = \frac{W_e}{W_{e,in}}$, was used to estimate the spreading of the erased patterns, where W_e and $W_{e,in}$ represent the FWHM of the erased patterns at $\tau = \tau_e$ and τ = 3 s, respectively (Figure 8B). Therefore, W_r > 1 means that the dimension of the erased patterns was larger than the pattern dimension for τ = 3 s. The W_r was <2 at all RH conditions for $\tau_e \leq$ 8 s; however, it was ~4 times larger for RH = 95% at τ_e = 60 s than the patterns

https://doi.org/10.1021/acs.langmuir.2c02096
Langmuir XXXX, XXX, XXX−XXX

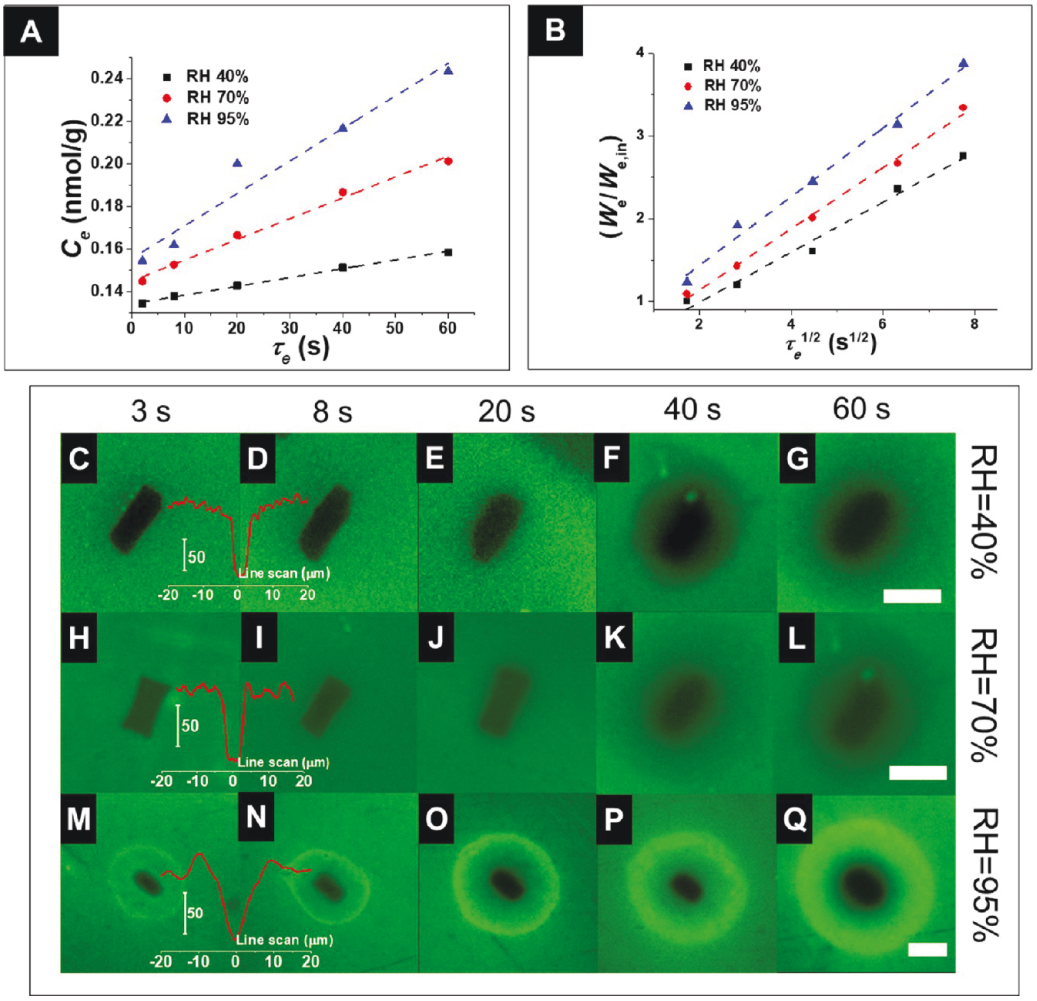

Figure 8. The dependence of the concentration of erased molecules as a function of τ_e (A) and normalized $\frac{W_e}{W_{e,in}}-\tau_e^{1/2}$ dependence at three RH conditions (B). Here, W_e and $W_{e,in}$ are the full width at half-maxima of the erased patterns at $t = \tau_e$ and 3 s, respectively. The fluorescence micrographs of erased patterns fabricated by PAAM PLEs with τ_e were 3 s (column 1), 8 s (column 2), 20 s (column 3), 40 s (column 4), and 60 s (column 5). The fluorescent micrographs contained in horizontal rows were obtained at RH = 40% (C−M); 70% (H−L); and 95% (M−Q). Scales for (C−G), (H−L), and (M−Q) are given in (G, L, Q), respectively. The scale bars in (G, L, J) were 10 μm.

obtained at τ_e = 3 s (Figure 8B). Higher humidity conditions and longer τ_e conditions facilitated the hydration of fluorescein molecules at the probe−substrate interface and in the vicinity of the meniscus, resulting in a much larger erasing size of the patterns. Interestingly, at RH = 95%, a bright circular ring at the periphery of the patterns was also observed for all dwell times investigated in the present studies (Figure 8M−Q). This observation likely originates from the formation of water droplets on the substrate close to the meniscus. It is known that the surface tension at the water droplet−air interface drives the dissolved molecules to the droplet edge, yielding the well-known coffee-ring structure after drying.[53] This coffee-ring effect becomes more significant at higher humidity, longer dwelling time, and larger contact area. The coffee-ring effect may negatively affect the pattern editing quality. Therefore, a strict control over RH, τ_e, and probe tip size should be considered for a desired application.

Fluorescence Emission Recovery after Erasing (FRAE). By tracking the changes in the fluorescence emission intensity of the erased spots as a function of time, recovery of emission in the erased patterns was observed. Figure S6 shows an increase in the emission intensity with time after patterns were erased with a PAAM probe (tip = 1 × 2 μm) at RH = 10 and 70%. We refer to this phenomenon as fluorescence emission recovery after erasing (FRAE). Although it is different in nature from the well-known phenomenon of fluorescence recovery after photobleaching (FRAP),[54] the overall characteristics of FRAE and FRAP are similar, where the emission recovery occurs with time. FRAE was quantified by monitoring taking the emission intensity profile of the erased pattern over time. Care was taken to minimize the effect of the exposure time and excitation intensity during the acquisition of fluorescence micrographs. Figure S6A,B shows the emission intensity line profiles of the pattern erased as a function of time for RH = 10 and 70%, respectively. Clearly, FRAE is more substantial at RH = 70% (Figure S6B) than at RH = 10% (Figure S6A). A quality factor, $f_r = \left(1 - \frac{I_t}{I_0}\right)$, was used to estimate the FRAE. Here, f_r is the fraction of fluorescence emission intensity recovered at time (τ_r), and I_0 and I_t are emission intensities of the erased patterns for τ_r = 0 s and τ_r = t, respectively. τ_r = 7200 s is considered the quasi-equilibrium FRAE time because the time required for half of the maximum recovery ($\tau_{r1/2}$) was ∼60 s for RH = 70%. The initial emission

https://doi.org/10.1021/acs.langmuir.2c02096
Langmuir XXXX, XXX, XXX−XXX

recovery was fast at RH = 70%, which was followed by a plateau. The estimated f_r = 41 and 5% were estimated at τ_r = 7200 s for RH = 70 and 10%, respectively (Figure S6C). Considering the low signal-to-noise-ratio for the emission signal at RH = 10%, f_r is considered negligible (Figure S6A). The FRAE equilibrium recovery depends on the diffusion and interaction of the fluorophores with water molecules present on the substrate. The mobility of the fluorophores on the PLE surface patterns is directional; that is, molecules move from the nonerased parts of the patterns (higher ink concentration) to the depleted parts of the patterns (lower ink concentration). Importantly, the movement of the fluorophores depends on local conditions, especially the RH of the experiments. At room temperature and low RH (10%), a clean glass-like surface can possess a sub-monolayer (sub-ML) of water where water is strongly bound to the surface.[45] At higher RH conditions (70%), however, the water layer is more than one ML and a large fraction of it is mobile "liquid-like" molecules.[45] The differences in water content and mobility of water molecules on the surface are likely to contribute to enhanced FRAE observed for experiments performed at RH = 70%. Therefore, fluorescein molecules diffused faster on liquid-like water due to higher mobility along with the presence of a larger quantity of mobile water molecules on the glass surface than those patterns at RH = 10%.

Large-Scale Complex Lithographic Editing Using PAAM PLEs. In practical probe-based lithography, molecular erasing frequently requires complex pattern editing. Different from the erasing process for simple patterns (such as dots or straight lines), the erasing process for complex patterns requires accurate registration of the PLE probes at various erasing positions during patterning. Furthermore, high editing efficiency and rapid recovery of the tip shape without significant distortion are also desired. To demonstrate erasing complex patterns with multiple probe−substrate contacts and lift-offs, we demonstrate erasing of a spiral pattern, Chinese characters, and an SIU pattern using a PAAM PLE (RH = 40%, probe dimension = 2 μm^2, and T = 22 °C) (Figure 9).

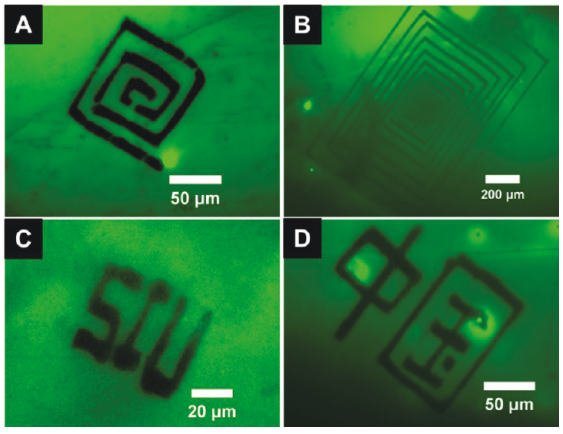

Figure 9. Demonstration of complex erasing patterns fabricated on a fluorescein-coated glass surface using a PAAM PLE probe. (A, B) Spiral erasing accomplished using a PAAM probe. The sharp turns in the erased patterns were almost right angles at each turn. (C) An "SIU" erasing pattern (scale bar 20 μm). (D) Chinese letter patterns were fabricated using a PLE probe (scale bar is 50 μm). The probe tip was 1 × 2 μm, speed of the probe = 5 μm/s, T = 22 °C, and RH = 40% for all the experiments.

Figure 9A shows that erasing of a spiral pattern of a total length of 720 μm with an average width of 10 μm was achieved in 20 s using a PAAM PLE. With the v_{probe} = 35 μm/s, the areal erasing rate (= probe−substrate contact width × speed of the probe) of 350 μm^2/s was achieved. The erasing speed for the spiral pattern in Figure 9B was accomplished with an average width of ∼20 μm with $r_e \approx$ 500 μm/s, yielding an areal erasing of 10,000 μm^2/s or 0.01 mm^2/s. Therefore, a pattern 20 μm wide and ∼2.3 cm long was accomplished in only ∼46 s, which is many orders of magnitude larger than the patterns reported in the literature.[26,27] The erasing efficiency was 92 and 90% at the beginning and end of the patterns respectively, and the patterns did not show any major defects. Surprisingly, the erasing track contains sharp and neat erasing boundaries at each turn, even at such a fast erasing rate. These experiments clearly demonstrate that soft polymeric probes with appropriate transporting media are suitably adaptive for large-area, high-speed, and high-definition microscale lithographic erasing. More complex patterns showing English and Chinese letters are shown in Figure 9C,D respectively.

An important point that needs to be mentioned here is that achieving such high erasing rates is enabled in part by fast solvation of the fluorescein dyes ($k_4 \gg 1$). As discussed earlier, the overall erasing kinetics requires that $\frac{(k_4k_5k_6k_7)}{k_{-7}} \gg 1$ (eq 3) so that probe-based erasing can be accomplished within the experimental time scale. Therefore, the erasing of the highly water-soluble dyes (fluorescein and rhodamine) at such a high speed is feasible within the time scale of the locomotion of the probes. On the other hand, the probe erasing rate would be many orders of magnitude lower for metal erasing (metal etching) or erasing of molecules where the dissolution rate of the species is much smaller in magnitude ($\frac{(k_4k_5k_6k_7)}{k_{-7}} \ll 1$). For example, the erasing of copper and silver was much slower than that of the fluorescent dye erasing obtained here.[28] In some cases, the metal etching rate was modulated using the etchant type and etchant concentration delivered by the PLE probes. For example, k_4 was significantly increased with a higher $FeCl_3$ concentration. Other experimental conditions such as RH, temperature, and etching promotors can also be tuned to increase the etching rate. By controlling the dimension and physical properties and experimental conditions, PLiSED may allow editing of patterns at the microscale, providing opportunities in a variety of applications.

CONCLUSIONS

We demonstrated simultaneous erasing and writing of two and three fluorescent molecules in one single step using locomotion of a probe over a surface. The pyramidal shaped nanoporous polymer probes were fabricated from an anisotropically etched Si template. Rapid erasing and writing of fluorescent molecules with high-definition patterns (smallest feature ∼3 μm) was accomplished using PAAM PLE probes. The erasing and writing efficiency of >95% was achieved under appropriate experimental conditions. The maximum areal erasing rate of 10,000 μm^2/s or 0.01 mm^2/s was demonstrated. The high erasing capacity (>26.2 mm^3 per gram of a PAAM) allowed a large erasing area of >0.22 mm^2. The cross-diffusion of two and three different types of fluorescent molecules allowed demonstration of simultaneous molecular erasing and deposition with high spatial accuracy and efficiency. The editing quality is dependent on experimental conditions such

https://doi.org/10.1021/acs.langmuir.2c02096
Langmuir XXXX, XXX, XXX−XXX

as RH, hydration degree of PLE, the porosity of PLE, and probe speed. The potential applications of simultaneous writing and erasing using probes include studies of surface chemical reactions, micro/nanoelectronics, biomolecular sensing, catalysis, and three-dimensional fabrication.

■ ASSOCIATED CONTENT

Supporting Information

The Supporting Information is available free of charge at https://pubs.acs.org/doi/10.1021/acs.langmuir.2c02096.

Materials and methods, fabrication of silicon template, Figures S1 to S6, and Tables S1 and S2 (PDF)

■ AUTHOR INFORMATION

Corresponding Author

Punit Kohli − *School of Chemical and Biomolecular Sciences, Southern Illinois University, Carbondale, Illinois 62901, United States;* orcid.org/0000-0003-3183-4385; Email: pkohli@chem.siu.edu

Authors

Kexin Jiao − *School of Chemical and Biomolecular Sciences, Southern Illinois University, Carbondale, Illinois 62901, United States;* Present Address: Present address: Applied Research Center, Florida International University, 10555 W Flagler Street, Miami, Florida 33174, USA

Nathalie Becerra-Mora − *School of Chemical and Biomolecular Sciences, Southern Illinois University, Carbondale, Illinois 62901, United States;* Present Address: Present address: Virginia-Maryland College of Veterinary Medicine, Virginia Tech, Blacksburg, Virginia 24060, USA

Brice Russell − *School of Physics and Applied Physics, Southern Illinois University, Carbondale, Illinois 62901, United States*

Aldo Migone − *School of Physics and Applied Physics, Southern Illinois University, Carbondale, Illinois 62901, United States*

Max E. Gemeinhardt − *School of Chemical and Biomolecular Sciences, Southern Illinois University, Carbondale, Illinois 62901, United States*

Boyd M. Goodson − *School of Chemical and Biomolecular Sciences and Materials Technology Center, Southern Illinois University, Carbondale, Illinois 62901, United States;* orcid.org/0000-0001-6079-5077

Complete contact information is available at: https://pubs.acs.org/10.1021/acs.langmuir.2c02096

Author Contributions

[+]K.J. and N.B.-M. contributed equally to the manuscript

Notes

The authors declare no competing financial interest.

■ ACKNOWLEDGMENTS

We would like to acknowledge the National Science Foundation (CHE-0748676 (P.K.) and CHE-1905341 (B.M.G.)) and the National Institutes of Health (GM 106364 (P.K.)) for the partial financial support of this research. We acknowledge the National Science Foundation for funding the purchase of scanning electron and atomic force microscopes through CHE-0959568 and CHE-1920255 awards, respectively. We acknowledge Dr. and Mrs. Gower for the financial support through the Gower fellowship to K.J. and N.B.M.

■ REFERENCES

(1) Piner, R. D.; Zhu, J.; Xu, F.; Hong, S.; Mirkin, C. A. "Dip-Pen" Nanolithography. *Science* **1999**, *283*, 661.

(2) Zhou, Y.; Xie, Z.; Brown, K. A.; Park, D. J.; Zhou, X.; Chen, P.-C.; Hirtz, M.; Lin, Q.-Y.; Dravid, V. P.; Schatz, G. C.; Zheng, Z.; Mirkin, C. A. Apertureless Cantilever-Free Pen Arrays for Scanning Photochemical Printing. *Small* **2015**, *11*, 913−918.

(3) Chen, C.; Zhou, X.; Xie, Z.; Gao, T.; Zheng, Z. Construction of 3D Polymer Brushes by Dip-Pen Nanodisplacement Lithography: Understanding the Molecular Displacement for Ultrafine and High-Speed Patterning. *Small* **2015**, *11*, 613−621.

(4) Zheng, Z.; Daniel, W. L.; Giam, L. R.; Huo, F.; Senesi, A. J.; Zheng, G.; Mirkin, C. A. Multiplexed Protein Arrays Enabled by Polymer Pen Lithography: Addressing the Inking Challenge. *Angew. Chem., Int. Ed.* **2009**, *48*, 7626−7629.

(5) Bian, S.; Zieba, S. B.; Morris, W.; Han, X.; Richter, D. C.; Brown, K.; Mirkin, C. A.; Braunschweig, A. B. Beam pen lithography as a new tool for spatially controlled photochemistry, and its utilization in the synthesis of multivalent glycan arrays. *Chem. Sci.* **2014**, 2023.

(6) Irvine, E. J.; Hernandez-Santana, A.; Faulds, K.; Graham, D. Fabricating protein immunoassay arrays on nitrocellulose using Dip-pen lithography techniques. *Analyst* **2011**, *136*, 2925−2930.

(7) Yu, Y.; Yan, C.; Zheng, Z. Polymer-Assisted Metal Deposition (PAMD): A Full-Solution Strategy for Flexible, Stretchable, Compressible, and Wearable Metal Conductors. *Adv. Mater.* **2014**, *26*, 5508−5516.

(8) Xie, Z.; Chen, C.; Zhou, X.; Gao, T.; Liu, D.; Miao, Q.; Zheng, Z. Massively Parallel Patterning of Complex 2D and 3D Functional Polymer Brushes by Polymer Pen Lithography. *ACS Appl. Mater. Interfaces* **2014**, *6*, 11955−11964.

(9) Eichelsdoerfer, D. J.; Brown, K. A.; Mirkin, C. A. Capillary bridge rupture in dip-pen nanolithography. *Soft Matter* **2014**, *10*, 5603−5608.

(10) Brown, K. A.; Eichelsdoerfer, D. J.; Shim, W.; Rasin, B.; Radha, B.; Liao, X.; Schmucker, A. L.; Liu, G.; Mirkin, C. A. A cantilever-free approach to dot-matrix nanoprinting. *Proc. Natl. Acad. Sci.* **2013**, *110*, 12921−12924.

(11) Eichelsdoerfer, D. J.; Brown, K. A.; Wang, M. X.; Mirkin, C. A. Role of Absorbed Solvent in Polymer Pen Lithography. *J. Phys. Chem. B* **2013**, *117*, 16363−16368.

(12) Zheng, Z.; Jang, J.-W.; Zheng, G.; Mirkin, C. A. Topographically Flat, Chemically Patterned PDMS Stamps Made by Dip-Pen Nanolithography. *Angew. Chem., Int. Ed.* **2008**, *47*, 9951−9954.

(13) Liu, G.; Petrosko, S. H.; Zheng, Z.; Mirkin, C. A. Evolution of Dip-Pen Nanolithography (DPN): From Molecular Patterning to Materials Discovery. *Chem. Rev.* **2020**, *120*, 6009−6047.

(14) Ginger, D. S.; Zhang, H.; Mirkin, C. A. The Evolution of Dip-Pen Nanolithography. *Angew. Chem., Int. Ed.* **2004**, *43*, 30−45.

(15) Yeshua, T.; Layani, M.; Dekhter, R.; Huebner, U.; Magdassi, S.; Lewis, A. Micrometer to 15 nm Printing of Metallic Inks with Fountain Pen Nanolithography. *Small* **2018**, *14*, 1702324.

(16) Salaita, K.; Wang, Y.; Mirkin, C. A. Applications of dip-pen nanolithography. *Nat. Nanotechnol.* **2007**, *2*, 145−155.

(17) Liu, G.; Hirtz, M.; Fuchs, H.; Zheng, Z. Development of Dip-Pen Nanolithography (DPN) and Its Derivatives. *Small* **2019**, *15*, 1900564.

(18) Brinkmann, F.; Hirtz, M.; Greiner, A. M.; Weschenfelder, M.; Waterkotte, B.; Bastmeyer, M.; Fuchs, H. Interdigitated Multicolored Bioink Micropatterns by Multiplexed Polymer Pen Lithography. *Small* **2013**, *9*, 3266−3275.

(19) Ma, H.; Jiang, Z.; Xie, X.; Huang, L.; Huang, W. Multiplexed Biomolecular Arrays Generated via Parallel Dip-Pen Nanolithography. *ACS Appl. Mater. Interfaces* **2018**, *10*, 25121−25126.

(20) Agusil, J. P.; Torras, N.; Duch, M.; Esteve, J.; Pérez-García, L.; Samitier, J.; Plaza, J. A. Highly Anisotropic Suspended Planar-Array

Chips with Multidimensional Sub-Micrometric Biomolecular Patterns. *Adv. Funct. Mater.* **2017**, *27*, 1605912.
(21) Vettiger, P.; Cross, G.; Despont, M.; Drechsler, U.; Durig, U.; Gotsmann, B.; Haberle, W.; Lantz, M. A.; Rothuizen, H. E.; Stutz, R.; Bining, G. K. The ″millipede″ - nanotechnology entering data storage. *IEEE Trans. Nanotechnol.* **2002**, *1*, 39−55.
(22) Haq, E. U.; Liu, Z.; Zhang, Y.; Ahmad, S. A.; Wong, L. S.; Armes, S. P.; Hobbs, J. K.; Leggett, G. J.; Micklefield, J.; Roberts, C. J.; Weaver, J. M. R. Parallel Scanning Near-Field Photolithography: The Snomipede. *Nano Lett.* **2010**, *10*, 4375−4380.
(23) Garcia, R.; Knoll, A. W.; Riedo, E. Advanced scanning probe lithography. *Nature Nanotech* **2014**, *9*, 577−587.
(24) Zhang, H.; Mirkin, C. A. DPN-Generated Nanostructures Made of Gold, Silver, and Palladium. *Chem. Mater.* **2004**, *16*, 1480−1484.
(25) Jang, J.-W.; Maspoch, D.; Fujigaya, T.; Mirkin, C. A. A "Molecular Eraser" for Dip-Pen Nanolithography. *Small* **2007**, *3*, 600−605.
(26) Becerra-Mora, N.; Rajasekaran, P. R.; Voss, K.-O.; Kollipara, V. K.; Kohli, P. Device fabrication on curvilinear two-dimensional surfaces using polymer probes. *Polymer* **2021**, *218*, No. 123521.
(27) Rajasekaran, P. R.; Zhou, C.; Dasari, M.; Voss, K. O.; Trautmann, C.; Kohli, P. Polymeric lithography editor: Editing lithographic errors with nanoporous polymeric probes. *Sci. Adv.* **2017**, *3*, No. e1602071.
(28) Becerra-Mora, N.; Vargas-Lizarazo, A. Y.; Orrison, C.; Barron, M.; Balaraman, R. P.; Kohli, P. Electrochemical Erasing Using a Polymer Lithography Editor for the Fabrication of Photoactive Devices. *ACS Appl. Electron. Mater.* **2019**, *1*, 752−763.
(29) Cho, S.; Hanif, Z.; Yun, Y.; Khan, Z. A.; Jang, S.; Ra, Y.; Lin, Z.-H.; La, M.; Park, S. J.; Choi, D. Triboelectrification-driven microbial inactivation in a conductive cellulose filter for affordable, portable, and efficient water sterilization. *Nano Energy* **2021**, *88*, No. 106228.
(30) Yun, Y.; Jang, S.; Cho, S.; Lee, S. H.; Hwang, H. J.; Choi, D. Exo-shoe triboelectric nanogenerator: Toward high-performance wearable biomechanical energy harvester. *Nano Energy* **2021**, *80*, No. 105525.
(31) Ra, Y.; La, M.; Cho, S.; Park, S. J.; Choi, D. Scalable Batch Fabrication of Flexible, Transparent and Self-triggered Tactile Sensor Array Based on Triboelectric Effect. *International Journal of Precision Engineering and Manufacturing-Green Technology* **2021**, *8*, 519−531.
(32) Choi, J. H.; Ra, Y.; Cho, S.; La, M.; Park, S. J.; Choi, D. Electrical charge storage effect in carbon based polymer composite for long-term performance enhancement of the triboelectric nanogenerator. *Composites Science and Technology* **2021**, *207*, No. 108680.
(33) Fregolente, P. B. L.; Maciel, M. R. W. Water Absorbing Material to Removal Water from Biodiesel and Diesel. *Procedia Engineering* **2012**, *42*, 1983−1988.
(34) Huang, C. J.; Su, Y. K.; Wu, S. L. The effect of solvent on the etching of ITO electrode. *Mater. Chem. Phys.* **2004**, *84*, 146−150.
(35) Donald, A. M. The use of environmental scanning electron microscopy for imaging wet and insulating materials. *Nat. Mater.* **2003**, *2*, 511−516.
(36) Emanuele, A. D.; Gilpin, C. Applications of the environmental scanning electron microscope to the analysis of pharmaceutical formulations. *Scanning* **1996**, *18*, 522−527.
(37) Chiu, Y.-C.; Kocagöz, S.; Larson, J. C.; Brey, E. M. Evaluation of Physical and Mechanical Properties of Porous Poly (Ethylene Glycol)-co-(L-Lactic Acid) Hydrogels during Degradation. *PLoS One* **2013**, *8*, No. e60728.
(38) Brunauer, S.; Emmett, P. H.; Teller, E. Adsorption of Gases in Multimolecular Layers. *J. Am. Chem. Soc.* **1938**, *60*, 309−319.
(39) Annabi, N.; Nichol, J. W.; Zhong, X.; Ji, C.; Koshy, S.; Khademhosseini, A.; Dehghani, F. Controlling the Porosity and Microarchitecture of Hydrogels for Tissue Engineering. *Tissue Eng., Part BTissue Engineering. Part B, Reviews* **2010**, *16*, 371−383.
(40) Chavda, H. V.; Patel, C. N. Effect of crosslinker concentration on characteristics of superporous hydrogel. *Int. J. Pharm. Invest.* **2011**, *1*, 17−21.
(41) Chern, J.-M.; Lee, W.-F.; Hsieh, M.-Y. Preparation and swelling characterization of poly (n-isopropylacrylamide)-based porous hydrogels. *J. Appl. Polym. Sci.* **2004**, *92*, 3651−3658.
(42) Anseth, K. S.; Bowman, C. N.; Brannon-Peppas, L. Mechanical properties of hydrogels and their experimental determination. *Biomaterials* **1996**, *17*, 1647−1657.
(43) Denisin, A. K.; Pruitt, B. L. Tuning the Range of Polyacrylamide Gel Stiffness for Mechanobiology Applications. *ACS Appl. Mater. Interfaces* **2016**, *8*, 21893−21902.
(44) Rozhok, S.; Piner, R.; Mirkin, C. A. Dip-Pen Nanolithography: What Controls Ink Transport? *J. Phys. Chem. B* **2003**, *107*, 751−757.
(45) Ewing, G. E. Ambient Thin Film Water on Insulator Surfaces. *Chem. Rev.* **2006**, *106*, 1511−1526.
(46) Sandrin, D.; Wagner, D.; Sitta, C. E.; Thoma, R.; Felekyan, S.; Hermes, H. E.; Janiak, C.; de Sousa Amadeu, N.; Kühnemuth, R.; Löwen, H.; Egelhaaf, S. U.; Seidal, C. A. M. Diffusion of macromolecules in a polymer hydrogel: from microscopic to macroscopic scales. *Phys. Chem. Chem. Phys.* **2016**, *18*, 12860−12876.
(47) Delamarche, E.; Schmid, H.; Bietsch, A.; Larsen, N. B.; Rothuizen, H.; Michel, B.; Biebuyck, H. Transport Mechanisms of Alkanethiols during Microcontact Printing on Gold. *J. Phys. Chem. B* **1998**, *102*, 3324−3334.
(48) Loh, O. Y.; Ho, A. M.; Rim, J. E.; Kohli, P.; Patankar, N. A.; Espinosa, H. D. Electric field-induced direct delivery of proteins by a nanofountain probe. *Proceedings of the National Academy of Sciences* **2008**, *105*, 16438.
(49) Bryce, C.; Berk, D. Kinetics of the dissolution of copper in iron(III) chloride solutions. *Ind. Eng. Chem. Res.* **1995**, *34*, 1412−1418.
(50) Burrows, W. H.; Lewis, C.; Saire, D. E.; Brooks, R. E. Briefs - ″Kinetics of the Copper-Ferric Chloride Reaction and the Effects of Certain Inhibitors″. *Phys. Chem. Chem. Phys.* **1964**, 79.
(51) Persson, I. Ferric Chloride Complexes in Aqueous Solution: An EXAFS Study. *J. Solution Chem.* **2018**, *47*, 797−805.
(52) Valiullin, R.; Kortunov, P.; Kärger, J.; Timoshenko, V. Concentration-dependent self-diffusion of liquids in nanopores: A nuclear magnetic resonance study. *J. Chem. Phys.* **2004**, *120*, 11804−11814.
(53) Deegan, R. D.; Bakajin, O.; Dupont, T. F.; Huber, G.; Nagel, S. R.; Witten, T. A. Capillary flow as the cause of ring stains from dried liquid drops. *Nature* **1997**, *389*, 827−829.
(54) Axelrod, D.; Koppel, D. E.; Schlessinger, J.; Elson, E.; Webb, W. W. Mobility measurement by analysis of fluorescence photobleaching recovery kinetics. *Biophys. J.* **1976**, *16*, 1055−1069.

https://doi.org/10.1021/acs.langmuir.2c02096
Langmuir XXXX, XXX, XXX−XXX